Enhanced piezoelectricity and modified dielectric screening of two-dimensional group-IV monochalcogenides

Lídia C. Gomes, A. Carvalho, and A. H. Castro Neto

Centre for Advanced 2D Materials and Graphene Research Centre, National University of Singapore, 6 Science Drive 2, 117546, Singapore

(Received 14 September 2015; revised manuscript received 16 November 2015; published 8 December 2015)

We use first-principles calculations to investigate the lattice properties of group-IV monochalcogenides. These include static dielectric permittivity, elastic and piezoelectric tensors. For the monolayer, it is found that the static permittivity, besides acquiring a dependence on the interlayer distance, is comparatively higher than in the 3D system. In contrast, it is found that elastic properties are little changed by the lower dimensionality. Poisson ratios relating in-plane deformations are close to zero, and the existence of a negative Poisson ratio is also predicted for the GeS compound. Finally, the monolayer shows piezoelectricity, with piezoelectric constants higher than those recently predicted to occur in other 2D systems, such as hexagonal BN and transition-metal dichalcogenide monolayers.

DOI: 10.1103/PhysRevB.92.214103 PACS number(s): 62.20.de, 62.20.dj, 77.84.Bw

I. INTRODUCTION

Piezoelectric materials are used in very diverse fields of application as sensors, actuators, electric field generators, and in general, any other applications requiring a conversion between electrical and mechanical energy. Recently, the availability of piezoelectric nanowires and nanobelts inspired the design of a class of "nanopiezotronic" devices which make use of both their piezoelectric and semiconducting properties [1]. These include, for example, nanogenerators, field-effect transistors, and piezoelectric diodes. Lead-free biocompatible piezoelectric materials are also sought as components for biomedical devices.

Piezoelectric crystals can also be found among two-dimensional (2D) materials. Some of these, like BN and 2H-stacked transition-metal dichalcogenides, are centrosymmetric in bulk form, but lose the inversion symmetry if the number of layers is odd. Exfoliation of W and Mo dichalcogenide monolayers thus produces 2D piezoelectric crystals with strain-induced polarization change in plane. This has been confirmed experimentally for MoS_2 by direct piezoresponse measurements and electrical characterization of MoS_2 devices under strain [2]. For a few transition-metal dichalcogenides, the in-plane d_{11} components of the piezoelectric tensor have been predicted to be superior to quartz [3].

Here, we concentrate on yet another family of layered materials that are piezoelectric in the monolayer form. These are the group-IV monochalcogenides SnS, GeS, SnSe, and GeSe [4]. Due to the hingelike structure similar to that of black phosphorus [5] (Fig. 1), group-IV monochalcogenides are very ductile along the direction perpendicular to the zigzags, stretching in that direction when out-of-plane strain is applied. Since the direction perpendicular to the zigzags is also the main polar direction, this results in a very large piezoelectric coefficient, exceeding by at least 1 order of magnitude that of other known 2D piezoelectrics.

In addition, group-IV monochalcogenides present a nearly vanishing or negative Poisson ratio. This is also a consequence of their anisotropic structure, as was recently reported [6] that a monolayer of black phosphorus (phosphorene) also possesses a negative Poisson ratio.

In this article, we use first-principles calculations to predict the lattice response properties of this family of materials, comprising a static dielectric constant, and elastic and piezoelectric constants.

A. Computational details

We use first-principles calculations to obtain the structural properties of monochalcogenides. We employ a first-principles approach based on Kohn-Sham density functional theory (KS-DFT) [7], as implemented in the Vienna *ab initio* simulation package (VASP) [8,9], which was used for calculation of elastic, piezoelectric, and static dielectric tensors. The core and valence electrons are treated with the projector-augmented wave (PAW) method [10].

The exchange correlation energy was described by the generalized gradient approximation (GGA) using the GGA–Perdew-Burke-Ernzerhof (PBE) [11] functional. For all materials, van der Waals interactions are taken into account by the method proposed by Tkatchenko and Scheffler [12] (TS), which presents a charge-density dependence of the dispersion coefficients and damping function. The Kohn-Sham orbitals were expanded in a plane-wave basis with a cutoff energy of 550 eV. The Brillouin zone (BZ) was sampled using a Γ-centered $1 \times 20 \times 20$ grid for the monolayers, following the scheme proposed by Monkhorst-Pack [13]. The results for bulk were obtained with a $6 \times 16 \times 16$ grid. Structural optimization has been performed with a very stringent tolerance of 0.001 eV/Å.

For comparison, we also performed calculations with the QUANTUM EXPRESSO code [14], in that case using Troullier-Martins pseudopotentials [15]. There was good agreement between the two codes whenever direct comparison could be established. All results shown were obtained with VASP, with the exception of the Poisson ratio calculations, which were performed with QUANTUM EXPRESSO to take advantage of the implementation of geometry optimization constraints.

The supercells are periodic in the monolayer plane, and large vacuum regions (>17 Å) are included to impose periodic boundary conditions in the perpendicular direction. Convergence tests with greater vacuum thickness were performed,

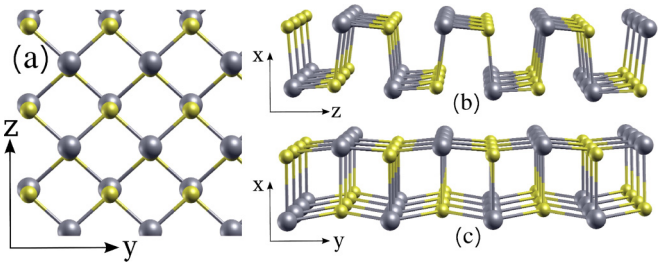

FIG. 1. (Color online) Structure of group-IV monochalcogenides: (a) top view and (b, c) side views of the monolayer unit cell, which are repeated along the x direction to obtain the bulk. The layers sit on the y-z plane, with the y axis parallel to the puckering direction.

and the values used are enough to avoid spurious interaction between neighboring images.

II. RESULTS

A. Structure

Bulk group-IV monochalcogenides SnS, SnSe, GeS, and GeSe have an orthorhombic structure with eight atoms per unit cell, four of each species. They belong to the space group $Pnma$. This structure is also known as the α phase of SnS, a naturally occurring mineral [16]. The waved structure adopted by these materials is similar to that of black phosphorus, with which these compounds are isoelectronic. All atoms are threefold coordinated and tetrahedral coordination results from the repulsion of the lone pairs. In the monolayer, the translational symmetry along the x direction is lost, and with it the inversion symmetry, and the resulting structure belongs to the $Pmn2_1$ space group. In this work, the axes system is chosen so that the layers sit on the y-z plane, with the y axis parallel to the puckering direction, as shown in Fig. 1. The layers are stacked together along the x axis to form the bulk.

The calculation of the lattice parameters of these materials, for both bulk and monolayer, have been discussed in previous theoretical studies [17–19], including our previous work, which employed the GGA-PBE approximation [4]. Since bulk group-IV monochalcogenides are van der Waals (vdW) bonded systems, in the current work we use vdW functionals as well. Table I presents the optimized lattice parameters for pure GGA and including vdW effects. Available experimental data for bulk SnS and SnSe are also included.

As should be expected, the most noticeable effects of vdW interactions in the structural parameters are on the lattice vector **a**, the one perpendicular to the plane of the layers in bulk. The inclusion of vdW forces results in values for **a** very close to the experimental data for bulk SnS and SnSe [20–22], with better results for the Tkatchenko-Scheffler method. The difference between GGA-PBE and vdW for monolayers is minor.

B. Static dielectric tensor

The static dielectric tensor ϵ is calculated from the force constant (**K**) and Born dynamical effective charge (BEC) (**Z**) tensors [23]:

$$\epsilon_{ij} = \epsilon_{ij}^{\infty} + V_0^{-1} Z_{mi} (K^{-1})_{mn} Z_{nj}. \quad (1)$$

TABLE I. Optimized lattice parameters (in Å) for the α phase of SnS, SnSe, GeS, and GeSe. We present results for GGA-PBE and including vdW by the Tkatchenko-Scheffler (TS) method. Experimental data for bulk SnS [20,21] and SnSe [22] are also presented.

		Monolayer		Bulk		
		b	**c**	**a**	**b**	**c**
SnS	GGA-PBE	4.07	4.24	11.37	4.02	4.35
	vdW-TS	4.08	4.25	11.12	4.00	4.27
	Expt.			11.20	3.98	4.33
SnSe	GGA-PBE	4.30	4.36	11.81	4.22	4.47
	vdW-TS	4.27	4.37	11.58	4.20	4.47
	Expt.			11.50	4.15	4.44
GeS	GGA-PBE	3.68	4.40	10.81	3.68	4.40
	vdW-TS	3.73	4.30	10.41	3.67	4.34
GeSe	GGA-PBE	3.99	4.26	11.31	3.91	4.45
	vdW-TS	4.00	4.22	10.93	3.90	4.39

The tensors **K** and **Z** are second derivative response functions and are calculated using density functional perturbation theory.

The electronic contribution ϵ_{ij}^{∞}, or ion-clamped static dielectric tensor, has been given in Ref. [4]. Here, we will concentrate on the lattice contribution, which for static electric fields, exceeds the electronic contribution.

For orthorhombic materials, the dielectric permittivity tensor has the form

$$\epsilon_{ij} = \begin{bmatrix} \epsilon_1 & 0 & 0 \\ 0 & \epsilon_2 & 0 \\ 0 & 0 & \epsilon_3 \end{bmatrix}, \quad (2)$$

where we have contracted a two-index into a one-index notation. The values calculated for bulk are given in Table II. While for the tin chalcogenides the calculated values are in excellent agreement with estimates obtained from comparing the LO-TO splitting of the vibrational bands with the dielectric constants obtained from reflectivity data, for the germanium chalcogenides there is some discrepancy. This can be due to many factors, including crystal quality. In particular, the dielectric response along the **x** axis is difficult to measure, explaining the range of variation of the measured values.

For two-dimensional materials, the dielectric constant is not well defined, depending on the interlayer distance L as [24–26]

$$\epsilon_i = \delta_i + \frac{4\pi \chi_i^{2D}}{L}, \quad (3)$$

where the 2D polarizability χ^{2D} (which includes both ionic and electronic contributions) is a constant and $\alpha,\beta = 2,3$, in accordance with our convention of the layers in the y-z plane. The $1/L$ dependence on the interlayer spacing of the electronic contribution to the susceptibility in the 2D systems has been verified in previous works [24–26]. In this work, we verified that the same behavior applies to the ionic contribution. In practice, this can be calculated using the same method as bulk [Eq. (1)] but replacing the volume by the area. The ionic contribution to χ^{2D} for the monolayers is given in Table II.

For comparison, if the interlayer distance L in the monolayer is taken to be the same as in bulk, the vdW-TS calculations for SnS results in static ionic contributions to

TABLE II. Ionic contributions to the 2D polarizability χ_2^{2D} and χ_3^{2D}, macroscopic static dielectric tensor components ϵ_2 and ϵ_3 for y and z directions of the monolayers, and ϵ_1, ϵ_2, and ϵ_3 for x, y, and z directions of bulk. Results for GGA-PBE and taking into account van der Waals interactions are included. Our calculations for the bulk can be compared to experimental values from previous works: (a) Ref. [27], (b) Ref. [28], (c) Ref. [29], and (d) Ref. [30].

		Monolayer				Bulk						
									Expt.			
		χ_2^{2D}	χ_3^{2D}	ϵ_2	ϵ_3	ϵ_1	ϵ_2	ϵ_3	ϵ_1	ϵ_2	ϵ_3	
SnS	GGA-PBE	35.8	21.5	78.0	50.1	14.9	31.7	18.3	16 ± 6	32 ± 7	18 ± 6	Ref. (a)
	vdW-TS	27.3	17.2	61.7	39.0	27.5	22.6	13.8	18.4	34.5	20.7	Ref. (d)
SnSe	GGA-PBE	73.6	26.4	156.5	56.0	21.3	39.1	12.1	26 ± 7	45 ± 8	32 ± 7	Ref. (a)
	vdW-TS	76.4	37.7	165.7	82.0	25.7	32.0	15.9	17.5	32.5	18.5	Ref. (d)
GeS	GGA-PBE	5.3	3.1	12.4	7.4	6.8	11.8	7.6	20.0	17.5	10.3	Ref. (b)
	vdW-TS	7.1	3.6	16.1	8.6	16.7	12.9	8.5	10.6	14.0	10.6	Ref. (d)
GeSe	GGA-PBE	24.0	7.7	53.3	17.1	6.9	12.3	5.7	11.3	8.5	3.2	Ref. (c)
	vdW-TS	28.6	10.1	65.7	24.3	14.3	15.7	7.7	9.7	12.5	9.6	Ref. (d)

the permittivity, with values 61 and 23, respectively, along the y direction, and 39 and 14, respectively, along the z direction, showing an increase of ~2.5 times when comparing the 2D and 3D systems. For SnSe and GeSe the ionic contribution to ϵ in monolayer reaches values three to four times higher than in their respective bulk forms. In the other hand, GeS presents just slightly higher values for ϵ from bulk to monolayer. The increase in the screening for SnS, SnSe, and GeSe can be explained by two factors: (i) increase in Born effective charges (BEC) and (ii) softening of polar modes due to the absence of interlayer binding. The increase in the BEC can be as high as 28% for SnS, SnSe, and GeSe, while for GeS $\mathbf{Z}$ differs by less than 3%. To have a better understanding of the contribution of lattice vibrational mode softening to the increase of the static dielectric constant, we consider the contribution of different modes to the components of the static dielectric tensor by writing ϵ_{ij} as in Refs. [31] and [32]:

$$\epsilon_{ij} = \epsilon_{ij}^{\infty} + \frac{4\pi}{V_0} \sum_m \frac{S_{m,ij}}{\omega_m^2}, \tag{4}$$

where V_0 is the volume of the cell. $S_{m,ij}$ is called the mode-oscillator strength of the ω_m mode along the $i,j(=x,y,z)$ directions of the material and it is related to the eigendisplacements $U_m(\kappa i)$ and Born effective charge tensors $Z^*_{\kappa,ii'}$ by

$$S_{m,ij} = \left(\sum_{\kappa i'} Z^*_{\kappa,ii'} U^*_{m,\mathbf{q}=0}(\kappa i') \right) \left(\sum_{\kappa' j'} Z^*_{\kappa',jj'} U_{m,\mathbf{q}=0}(\kappa' j') \right), \tag{5}$$

where κ is the index for the ions in the primitive cell. The ionic contribution to ϵ is then given by the second term in the right side of Eq. (4). The expression for $S_{m,\alpha\beta}$ shows that an increase in the BEC increases the contribution of the ionic part of ϵ. However, the dominant contribution comes from the ω_m modes. In Table III we present the frequency of the modes with a major contribution to the static dielectric constant for monolayer and bulk monochalcogenides along the in-plane directions. For all materials, just one mode contributes significantly to the yy component of ϵ, while there are two modes which contribute almost equally to the zz components in bulk SnS and monolayer and bulk SnSe and GeSe. A significant softening of the contributing modes occurs when going from 3D to 2D forms, probably due to the lack of interaction with upper and bottom layers, observed in bulk. SnSe presents the largest softening in the contributing modes, with $\omega_m^{3D}/\omega_m^{2D} = 1.9$ along the y direction up to $\omega_m^{3D}/\omega_m^{2D} = 2.5$ along z. GeS, however, presents the smallest softening of the modes, where we have $\omega_m^{3D}/\omega_m^{2D} = 1.1$ and 1.5 for the contribution to the yy and zz components of ϵ.

C. Elastic constants and Poisson ratio

1. Elastic constants

The elastic constant (stiffness) tensor is defined in the linear regime by Hooke's law,

$$\sigma_i = C_{ij}\varepsilon_j, \tag{6}$$

where σ and ε are the stress and strain tensors, respectively, and C_{ij} are the elastic constants. In this equation, and the following, there is an implicit sum over repeated indexes. Numerically, the elastic constants are easily determined using the equation of state. The change in the total energy $E(V_0)$ of a system due to an external strain (ε) is given by

$$E(V_0,\varepsilon) = E(V_0) + \frac{V_0}{2} C_{ij}\varepsilon_i\varepsilon_j, \tag{7}$$

TABLE III. Modes (cm^{-1}) at $\mathbf{q} = 0$ with the largest contribution to the static dielectric tensors ϵ_2 and ϵ_3 (in Voigt notation), as defined in Eq. (4), for the y and z directions. For bulk SnS and monolayer and bulk SnSe and GeSe, the two modes presented in the table contribute almost equally to the ϵ_3 component. The presented values are obtained considering vdW interactions and do not take into account LO-TO splitting effects.

	ϵ_2		ϵ_3	
	Monolayer	Bulk	Monolayer	Bulk
SnS	104	158	62	102/189
SnSe	53	102	56/78	132/86
GeS	180	207	77	116
GeSe	94	145	137/76	184/87

TABLE IV. Calculated clamped-ion (C-i) and relaxed-ion (R-i) components of the elastic tensor C_{ij} for bulk and monolayer. The elastic constants for the monolayer assume an effective layer thickness $d_0 = a/2$ to allow direct comparison with bulk. All values are given in 10^{10} N/m^2.

			Monolayer								
			C_{11}	C_{22}	C_{33}	C_{12}	C_{13}	C_{23}	C_{44}	C_{55}	C_{66}
SnS	GGA-PBE	C-i		9.59	8.81			5.68	5.50		
		R-i		7.59	3.67			3.19	3.44		
	vdW-TS	C-i		9.65	9.29			5.70	5.25		
		R-i		7.72	3.85			2.68	2.81		
SnSe	GGA-PBE	C-i		7.90	7.26			4.54	4.81		
		R-i		6.92	3.32			2.77	2.32		
	vdW-TS	C-i		5.68	5.34			2.96	3.28		
		R-i		5.04	2.89			1.83	1.80		
GeS	GGA-PBE	C-i		9.51	8.92			6.08	5.41		
		R-i		8.48	2.82			4.00	3.44		
	vdW-TS	C-i		9.41	9.25			6.17	5.52		
		R-i		8.26	3.02			3.93	3.49		
GeSe	GGA-PBE	C-i		9.78	8.46			5.34	6.00		
		R-i		8.87	3.59			3.44	4.10		
	vdW-TS	C-i		10.19	9.37			5.42	6.04		
		R-i		9.19	4.41			3.40	3.81		
			Bulk								
			C_{11}	C_{22}	C_{33}	C_{12}	C_{13}	C_{23}	C_{44}	C_{55}	C_{66}
SnS	GGA-PBE	C-i	12.12	9.53	8.31	2.45	2.56	5.51	5.29	2.56	2.43
		R-i	4.85	7.99	3.42	1.31	1.80	3.16	3.47	1.95	2.00
	vdW-TS	C-i	12.15	9.68	8.79	2.64	3.07	5.59	5.37	3.15	2.74
		R-i	6.59	7.70	3.84	1.86	2.66	2.80	3.24	2.87	2.50
SnSe	GGA-PBE	C-i	10.99	8.39	7.61	1.76	2.03	5.09	5.20	1.93	1.77
		R-i	4.35	6.93	3.48	0.74	1.23	2.99	3.32	1.37	1.07
	vdW-TS	C-i	11.72	9.30	8.29	1.87	2.44	5.23	5.40	2.44	1.97
		R-i	6.09	7.49	4.27	0.99	2.12	2.86	3.29	2.09	1.24
GeS	GGA-PBE	C-i	12.40	10.47	8.83	2.79	2.67	6.00	5.75	3.18	2.93
		R-i	3.71	8.96	3.02	0.97	0.72	3.31	3.65	1.69	1.73
	vdW-TS	C-i	12.84	10.93	9.48	2.72	2.91	5.94	6.13	3.61	3.35
		R-i	5.31	8.94	3.41	1.11	1.44	2.81	3.76	2.90	2.51
GeSe	GGA-PBE	C-i	12.14	10.47	8.59	1.98	2.05	6.45	6.52	2.43	2.42
		R-i	3.20	8.72	3.75	0.29	0.82	3.91	3.93	1.15	0.96
	vdW-TS	C-i	12.53	10.02	8.63	1.73	2.22	5.64	5.67	2.92	2.44
		R-i	4.16	8.06	3.85	0.26	1.38	3.05	3.50	2.08	0.88

where V_0 is the volume of the unstrained material. Here, the electric field term vanishes because of the periodic boundary conditions ($d\vec{E} = 0$). For the monolayer system, the area (A_0) should figure instead. However, to facilitate the comparison with 3D systems and previous calculations [33], we use an effective thickness d_0. The most obvious choice is to take d_0 to be the distance between the layers in bulk, as is common practice in graphene [34].

Symmetry imposes restrictions on the number of nonzero components C_{ij}. Both for bulk and monolayer there are nine independent nonvanishing elements C_{ij} (in Voigt notation):

$$C_{ij} = \begin{bmatrix} C_{11} & C_{12} & C_{13} & 0 & 0 & 0 \\ C_{12} & C_{22} & C_{23} & 0 & 0 & 0 \\ C_{13} & C_{23} & C_{33} & 0 & 0 & 0 \\ 0 & 0 & 0 & C_{44} & 0 & 0 \\ 0 & 0 & 0 & 0 & C_{55} & 0 \\ 0 & 0 & 0 & 0 & 0 & C_{66} \end{bmatrix}. \quad (8)$$

However, we will consider that the monolayers are ideal 2D systems, with only in-plane stress. This excludes the elastic constants coupling ε_i to σ_6 and σ_5 (this is equivalent to σ_{12} and σ_{13}). Since in the absence of an external torque, the σ tensor is symmetrical and the only relevant elements are (in Voigt notation) C_{22}, C_{33}, C_{23}, and C_{44}.

The elastic constants for the monolayer were obtained from Eq. (6), applying finite distortions to the supercell. The stress components σ_{2i} and σ_{3i} are calculated using the effective thickness d_0 to define the lateral area of the layers. We have calculated C_{ij} both in clamped-ion and relaxed-ion conditions by fixing the atomic coordinates or allowing them to relax, respectively, for each distortion of the lattice vectors. The results for bulk and monolayer group-IV monochalcogenides are presented in Table IV for calculations with and without vdW effects. Using the definition of d_0, the elastic constants are of the same order of magnitude for monolayer and bulk. In most cases, though, they are slightly higher for the bulk for

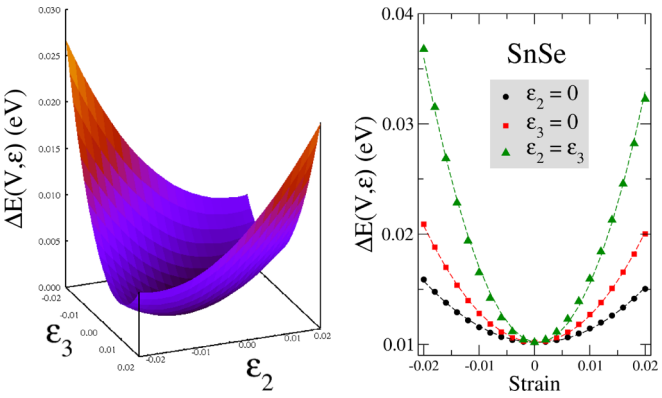

FIG. 2. (Color online) The three-dimensional surface plot of total energy (in eV) versus uniaxial strain along y and z directions of a SnSe monolayer. Projections on the $\varepsilon_2 = 0$, $\varepsilon_3 = 0$, and $\varepsilon_2 = \varepsilon_3$ planes show the quadratic dependence of the energy of the system to the applied strain, from where the elastic constants can also be calculated.

both relaxed and clamped-ion coefficients, indicating that the monolayers are less stiff for in-plane deformations. The main effects of vdW interactions in bulk are observed in the elastic constant components related to the x direction of the materials (those with indices $1j, j = 1,2,3$ as well as 55 and 66). The C_{11} constants are the most affected by the vdW forces, as expected, and differences of up to 50% are observed when compared to the GGA-PBE results.

Figure 2 shows the total energy versus strain along the y and z directions for a SnSe monolayer. The quadratic dependence of energy to the applied strain and the anisotropy between the perpendicular in-plane directions of the layer is given by

$$\Delta E(V,\varepsilon) = \frac{V_0}{2}\left(C_{22}\varepsilon_2^2 + C_{33}\varepsilon_3^2\right) + V_0 C_{23}\varepsilon_2\varepsilon_3, \qquad (9)$$

where $\Delta E(V,\varepsilon) = E(V,\varepsilon) - E(V_0,\varepsilon = 0)$ and $C_{32} = C_{23}$. The results for SnS, GeS, and GeSe are very similar, differing only in the ratio between elastic constants.

It is also noteworthy that C_{22} (the elastic constant for the zigzag direction) is much lower for group-IV monochalcogenides than for black phosphorus (18.6×10^{10} N/m^2), in contrast with other elastic constant elements which are little changed [35].

2. *Young modulus and Poisson ratio*

The Young modulus and Poisson ratio are derived mechanical properties that can give direct information on how a system behaves under uniaxial stress, i.e., when $\sigma_i \neq 0$ and $\sigma_j = 0$ for all $j \neq i$. Here, we calculate these moduli to highlight the role of anisotropy on the mechanical response of group-IV monochalcogenides.

We define the Young modulus as

$$Y^i = \frac{\partial \sigma_i}{\partial \varepsilon_i}. \qquad (10)$$

Since the materials in consideration here are orthorhombic and the choice of principal direction is arbitrary, i can be any of the principal directions of the crystal. Similarly, we define multiple Poisson ratios ν_{ij}, corresponding to the negative ratio of the strain response at a direction i to the strain applied along a transversal direction j:

$$\nu_{ij} = -\frac{\partial \varepsilon_i}{\partial \varepsilon_j}, \qquad (11)$$

for $i \neq j$.

In order to calculate the Poisson ratio and Young's modulus of monolayer monochalcogenides, according to Eqs. (10) and (11), strains from -6% to 6% were applied in the in-plane and out-of-plane directions of the layers. The results are presented in Table V, for GGA-PBE calculations and including vdW effects.

As the elastic constants of single layers are not considerably modified by introduction of vdW effects (Table IV), we should also expect small changes in the Poisson ratio, which is confirmed in the results presented in Table V. Most of the materials have a positive Poisson ratio, which means that when a compressive strain is applied along one direction, the others expand. Conversely, if the material is stretched along one direction, it will compress along the perpendicular directions. This due to the materials' tendency to conserve their volume. However, since group-IV monochalcogenides are very anisotropic, the values for the Poisson ratio vary greatly for different combinations of directions i, j.

This is apparent in Fig. 3, which illustrates the response of the monolayers under uniaxial stress, including vdW interactions. First, it is clear that the linear region where the

TABLE V. Poisson's ratio and Young's modulus (in GPa) for the monolayer monochalcogenides for GGA-PBE and including vdW effects. The data for monolayer phosphorene from Refs. [6] and [33] are included for comparison. b/c is the ratio between in-plane lattice parameters.

		ε_1		ε_2		ε_3					
		ν_{21}	ν_{31}	ν_{12}	ν_{32}	ν_{13}	ν_{23}	b/c	Y_1	Y_2	Y_3
SnS	GGA-PBE	0.097	0.277	0.025	0.861	0.067	0.419	0.97	32.4	15.1	8.7
	vdW-TS	0.101	0.284	0.022	0.894	0.075	0.422	0.96	32.4	15.4	7.1
SnSe	GGA-PBE	0.120	0.153	0.046	0.733	0.065	0.474	0.99	30.4	16.2	11.3
	vdW-TS	0.131	0.173	0.046	0.709	0.069	0.486	0.98	31.2	16.3	11.4
GeS	GGA-PBE	−0.214	0.940	−0.137	1.512	0.126	0.451	0.84	26.8	7.8	2.2
	vdW-TS	−0.190	0.987	−0.194	1.590	0.167	0.409	0.87	22.2	8.4	1.8
GeSe	GGA-PBE	0.128	0.181	0.051	0.919	0.068	0.389	0.94	30.2	15.9	7.9
	vdW-TS	0.126	0.194	0.037	0.980	0.079	0.384	0.95	30.0	15.7	7.5
P	GGA-PBE			−0.027	0.930	0.046	0.400	0.88	44.0	166.0	

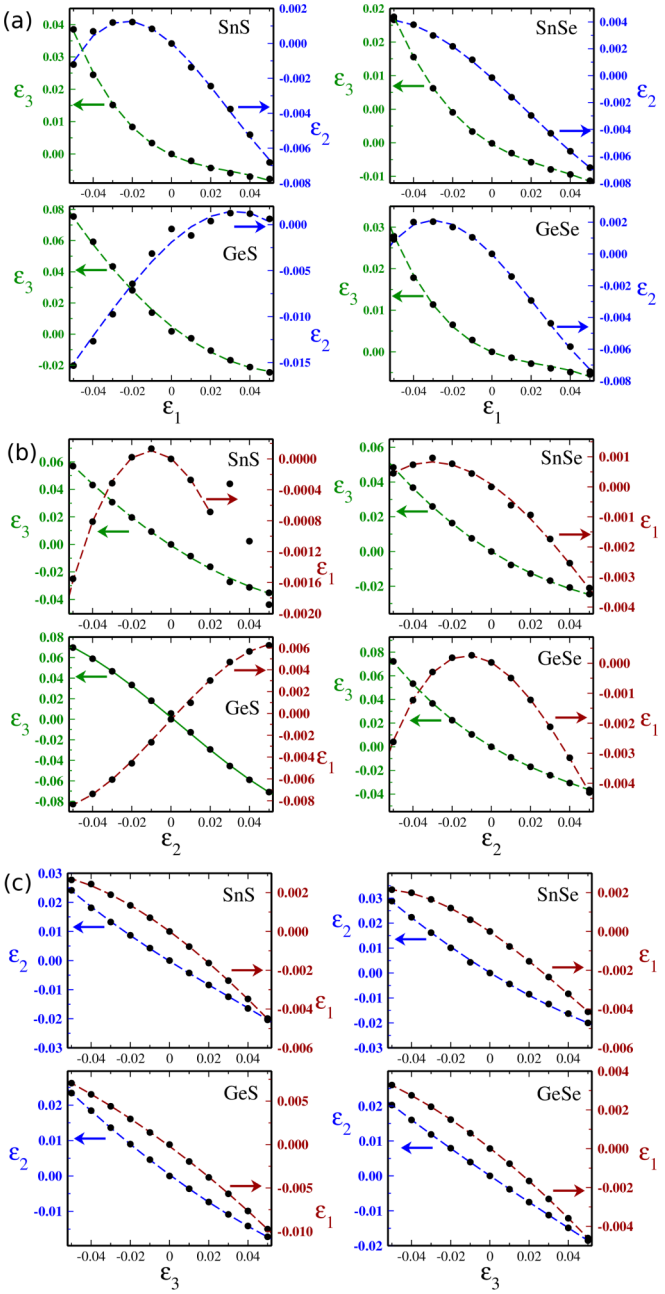

FIG. 3. (Color online) Response of monolayer monochalcogenides under uniaxial stress along (a) x, (b) y, and (c) z directions of the layers, including vdW effects. Strain components for the directions perpendicular to the external force are plotted as a function of the strain component along the direction of the external force.

Young modulus and Poisson ratio given by Eqs. (10) and (11) are constant is quite narrow, in some cases less than 2% strain.

In particular, if $i = 1$ or $j = 1$, the Poisson ratio is very close to zero, indicating that distortion along the in-plane directions and the direction perpendicular to the plane are practically decoupled. A very interesting exception is found in GeS: this is the only material in group-IV monochalcogenides that shows a negative linear Poisson ratio in the out-of-plane x direction. The calculated value of $\nu_{12} = -0.137$ for GeS is

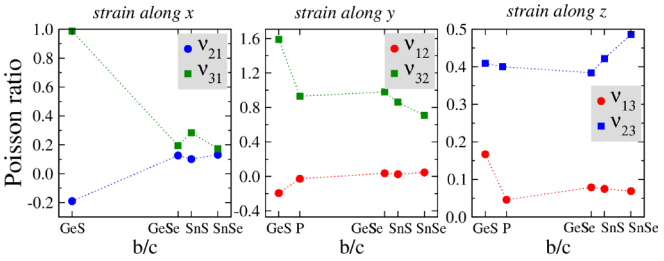

FIG. 4. (Color online) Poisson ratio (with vdW correction) versus the degree of anisotropy, given by the ratio between in-plane lattice constants b and c, for monolayer crystals. The values for phosphorene (P) taken from Ref. [6] are also included.

about 5 times larger than the value calculated for phosphorene in Ref. [6], which reports $\nu_{12} = -0.027$ for this material.

In contrast, the ratios ν_{23} and ν_{32} for the in-plane uniaxial stress are in the ranges 0.3–0.5 and 0.7–1.6. The Poisson ratio is intrinsically linked with the anisotropy. In plotting the Poisson ratio against the anisotropy of the monolayer crystals (b/c), it becomes evident why GeS departs from the other materials (Fig. 4). Among all four materials, GeS has the smallest b/c ratio and is located far away from GeSe, SnS, and SnSe. This behavior is more evident in the plot of ν_{21} and ν_{31} (left panel in Fig. 4), obtained by applying uniaxial strain in the out-of-plane x direction.

It is worth commenting on the behavior of monolayer SnS under tensile strain ($\epsilon > 0$) along the y direction. Calculations with vdW interactions show a "discontinuity" in the response of ϵ_1 at $\epsilon_2 \sim 3\%$ [upper-left panel in Fig. 3(b)], an indication of structural transition. Indeed, an analysis of the optimized strained structures shows that the initially unbonded Sn and S atoms along z [Fig. 1(b)] establish ionic bonds for tensile strain $\epsilon_2 > 3\%$, and the structure gains a mirror symmetry in the x-z plane. The opposite occurs along the y direction, where alternating Sn and S atoms become unbonded and lose the mirror symmetry, in response to the external stress. The same scenario is expected for the other three materials, probably occurring for strain values out of the range considered in this paper. A more detailed analysis of structural transitions on these materials is left for a further work.

D. Piezoelectric tensor

Noncentrosymmetric crystals display a change of polarization P_i under mechanical stress:

$$P_i = d_{ij}\sigma_j. \tag{12}$$

Equation (12) shows that application of a stress σ_j along the j direction of a piezoelectric material induces a change of polarization of magnitude P_i in its i direction. P_i is related to σ_j by a piezoelectric tensor with components d_{ij}. This is known as the direct piezoelectric effect. In the same way, the converse piezoelectric effect occurs when a strain ε is induced in a material under an external electric field. The converse effect can be written:

$$\varepsilon_j = d_{ij}E_i, \tag{13}$$

where E_i is the component of the applied electric field in the i direction. The piezoelectric coefficients d_{ij} in Eqs. (12)

TABLE VI. Nonzero ion-clamped and relaxed-ion piezoelectric coefficients (10^{-10} C/m). The tensor components are calculated according to $e^0_{ij} = -\frac{\partial \sigma_i}{\partial E_j}$, where the values for the other 2D materials h-BN, MoS_2, and $MoTe_2$ are taken from Ref. [3] and included for comparison.

		Clamped-ion			Relaxed-ion		
		e^{2D}_{32}	e^{2D}_{33}	e^{2D}_{24}	e^{2D}_{32}	e^{2D}_{33}	e^{2D}_{24}
SnS	GGA-PBE	−4.73	0.29	−4.39	0.76	23.36	15.70
	vdW-TS	−5.01	0.47	−4.75	2.27	18.94	15.54
SnSe	GGA-PBE	−4.89	0.53	−4.67	4.42	24.18	28.17
	vdW-TS	−4.67	0.58	−4.29	6.73	30.25	30.82
GeS	GGA-PBE	−6.69	−1.25	−7.10	−4.97	7.28	0.37
	vdW-TS	−6.89	−0.81	−7.08	−4.64	8.83	2.05
GeSe	GGA-PBE	−7.16	−0.26	−7.37	−3.00	13.26	8.25
	vdW-TS	−7.11	0.35	−7.20	−1.48	16.95	12.48
h-BN		−3.71	3.71		−1.38	1.38	
MoS_2		−3.06	3.06		−3.64	3.64	
$MoTe_2$		−2.98	2.98		−5.43	5.43	

and (13) are the same, and the proof of such equality is based on thermodynamical arguments [36]. In addition, other piezoelectric coefficients can be defined, for example, e_{ij}, that directly relates E and σ, by

$$e_{ij} = -\frac{\partial \sigma_i}{\partial E_j} = \frac{\partial P_i}{\partial \varepsilon_j}. \tag{14}$$

For a constant electric field, the piezoelectric tensors d_{ij} and e_{ij} are related via the elastic tensor C_{ij} as

$$e_{ij} = \sum_{k=1}^{6} d_{ik} C_{kj}. \tag{15}$$

However, in the case of a 2D system it is more meaningful to define a 2D polarization per unit area, P_i^{2D}. Thus, we redefine e^{2D}_{ij},

$$e^{2D}_{ij} = \frac{\partial P_i^{2D}}{\partial \varepsilon_j}. \tag{16}$$

The number of nonzero coefficients e^{2D}_{ij} is completely defined by the symmetry of the system. The layered group-IV monochalcogenides are centrosymmetric in bulk (and even-numbered layers) and therefore are not piezoelectric. However, single layers belong to the polar space group $Pmn2_1$. In this space group, there are five nonzero piezoelectric constants, e^{2D}_{15}, e^{2D}_{24}, e^{2D}_{31}, e^{2D}_{32}, and e^{2D}_{33}, where we use Voigt notation [36], with 1, 2, and 3 corresponding to the x, y, and z directions, respectively [37]. As for the calculation of the elastic constants, we consider only in-plane strain components for computation of the e^{2D}_{ij} constants, which limits our discussion to e^{2D}_{32}, e^{2D}_{33}, and e^{2D}_{24}. The calculated values are presented in Table VI.

$$e^{2D}_{ij} = \begin{bmatrix} 0 & 0 & 0 & 0 & e^{2D}_{15} & 0 \\ 0 & 0 & 0 & e^{2D}_{24} & 0 & 0 \\ e^{2D}_{31} & e^{2D}_{32} & e^{2D}_{33} & 0 & 0 & 0 \end{bmatrix} \tag{17}$$

To the best of our knowledge, there is still no experimental data on the piezoelectric properties of few-layers group-IV monochalcogenides with an odd number of layers. However, we take for comparison single-layer transition metal dichalcogenides (TMDCs) and hexagonal boron nitride (h-BN), of which piezoelectric coefficients have been theoretically calculated [3], and the object of recent experimental measurements [2].

Similar to h-BN and TMDC [3], the piezoelectric elements e_{32}, e_{33}, and e_{24} of group-IV monochalcogenides are enhanced as we move downward in the periodic table. The value of e_{33} (for both the relaxed and clamped-ion case) seems also to be directly related to the degree of anisotropy of the materials, as given by the ratio between in-plane lattice parameters b/c.

For SnS and SnSe, e_{33} is 1 order of magnitude higher than for other known 2D piezoelectric materials. This element relates the polarization along the z direction, the polar direction of the crystal, with the strain along the same direction. Since, as we have discussed before, this structure is extremely ductile along the z direction, the corresponding piezoelectric response is very large.

The very large e_{33} coefficient found in our calculations is in line with the result recently reported in Ref. [38], which also investigates piezoelectric properties of monochalcogenides. However, there are quantitative differences in some of the elements, which may be due to the method used and to the anharmonicity of the material.

It is also instructive to compare the piezoelectric coefficients of group-IV monochalcogenides with typical 3D piezoelectric materials. Employing once again the definition of an effective thickness d_0, we obtain $e_{33} = 4.11$, 4.26, 1.36, and 2.37 C/m^2 for SnS, SnSe, GeS, and GeSe, respectively. These coefficients are 1–2 orders of magnitude higher than the piezoelectric coefficients of the α quartz and four of its homeotypes MXO_4 (M = Al, Ga, Fe; X = P, As) [39].

III. CONCLUSIONS

The group-VI monochalcogenides SnS, SnSe, GeS, and GeSe have an orthorhombic structure similar to phosphorene. This structure results in in-plane anisotropy of the static permittivity, elastic constants, and piezoelectric coefficients. In this study, we investigated those properties both for monolayer and bulk systems by including van der Waals effects, highlighting the differences resulting from the lower dimensionality. The electric susceptibility in the 2D systems is known to have a $1/L$ dependence on the interlayer spacing [24]. This has been verified for electronic contribution to the low-frequency susceptibility [25]. In this work, we verified numerically that the same applies to the ionic contribution. However, if we extrapolate the ionic contribution of the 2D permittivity to $L = a/2$, where $a/2$ is the interlayer spacing in bulk, we notice a great enhancement for SnS, SnSe, and GeSe. This is mainly due to the larger softening of the modes in the 2D systems, but is also partially accounted for by the effective Born charges in the 2D material.

In contrast, elastic constants remain nearly unchanged in monolayer, compared to bulk, if an equivalent volume of material is considered. The most remarkable among the elastic properties of group-VI monochalcogenides is the Poisson ratios. The Poisson ratio ν_{12} and ν_{21}, relating strain and uniaxial strain for the direction perpendicular to the plane

and the armchair in-plane direction, are very small or even negative for GeS, the most anisotropic among the four materials.

Finally, while in bulk the presence of inversion symmetry forbids piezoelectricity, in monolayer there is one polar direction coinciding with the C_2 axis (z). Piezoelectric constants are higher than those recently predicted to occur in other 2D systems, such as hexagonal BN and transition-metal dichalcogenide crystals.

ACKNOWLEDGMENTS

This work was supported by the National Research Foundation-Prime Ministers Office, Republic of Singapore, under its Medium Sized Centre Programme and CRP award "Novel 2D materials with tailored properties: beyond graphene" (Grant No. R-144-000-295-281). The first-principles calculations were carried out at the GRC high-performance computing facilities.

[1] Z. L. Wang, Adv. Mater. **19**, 889 (2007).
[2] W. Wu, L. Wang, Y. Li, F. Zhang, L. Lin, S. Niu, D. Chenet, X. Zhang, Y. Hao, T. F. Heinz, J. Hone, and Z. L. Wang, Nature (London) **514**, 470 (2014).
[3] K.-A. N. Duerloo, M. T. Ong, and E. J. Reed, J. Phys. Chem. Lett. **3**, 2871 (2012).
[4] L. C. Gomes and A. Carvalho, Phys. Rev. B **92**, 085406 (2015).
[5] Z. Zhu, J. Guan, D. Liu, and D. Tomnek, ACS Nano **9**, 8284 (2015).
[6] J.-W. Jiang and H. S. Park, Nat. Commun. **5**, 4727 (2014).
[7] W. Kohn and L. J. Sham, Phys. Rev. **140**, A1133 (1965).
[8] G. Kresse and J. Furthmller, Comput. Mater. Sci. **6**, 15 (1996).
[9] G. Kresse and J. Furthmüller, Phys. Rev. B **54**, 11169 (1996).
[10] P. E. Blöchl, Phys. Rev. B **50**, 17953 (1994).
[11] J. P. Perdew, K. Burke, and M. Ernzerhof, Phys. Rev. Lett. **77**, 3865 (1996).
[12] A. Tkatchenko and M. Scheffler, Phys. Rev. Lett. **102**, 073005 (2009).
[13] H. J. Monkhorst and J. D. Pack, Phys. Rev. B **13**, 5188 (1976).
[14] P. Giannozzi *et al.*, J. Phys.: Condens. Matter **21**, 395502 (2009).
[15] N. Troullier and J. L. Martins, Phys. Rev. B **43**, 1993 (1991).
[16] A. Walsh and G. W. Watson, Phys. Rev. B **70**, 235114 (2004).
[17] G. A. Tritsaris, B. D. Malone, and E. Kaxiras, J. Appl. Phys. **113**, 233507 (2013).
[18] J. Vidal, S. Lany, M. d'Avezac, A. Zunger, A. Zakutayev, J. Francis, and J. Tate, Appl. Phys. Lett. **100**, 032104 (2012).
[19] S. Alptekin and M. Durandurdu, Solid State Commun. **150**, 870 (2010).
[20] H. Wiedemeier and H. G. Schnering, Z. Kristallogr. **156**, 143 (1981).
[21] L. Ehm, K. Knorr, P. Dera, A. Krimmel, P. Bouvier, and M. Mezouar, J. Phys.: Condens. Matter **16**, 3545 (2004).
[22] I. Lefebvre, M. A. Szymanski, J. Olivier-Fourcade, and J. C. Jumas, Phys. Rev. B **58**, 1896 (1998).
[23] X. Wu, D. Vanderbilt, and D. R. Hamann, Phys. Rev. B **72**, 035105 (2005).
[24] P. Cudazzo, I. V. Tokatly, and A. Rubio, Phys. Rev. B **84**, 085406 (2011).
[25] T. C. Berkelbach, M. S. Hybertsen, and D. R. Reichman, Phys. Rev. B **88**, 045318 (2013).
[26] D. Warschauer, J. Appl. Phys. **34**, 1853 (1963).
[27] H. R. Chandrasekhar, R. G. Humphreys, U. Zwick, and M. Cardona, Phys. Rev. B **15**, 2177 (1977).
[28] J. D. Wiley, W. J. Buckel, and R. L. Schmidt, Phys. Rev. B **13**, 2489 (1976).
[29] H. R. Chandrasekhar and U. Zwick, Solid State Commun. **18**, 1509 (1976).
[30] L.-M. Yu, A. Degiovanni, P. A. Thiry, J. Ghijsen, R. Caudano, and Ph. Lambin, Phys. Rev. B **47**, 16222 (1993).
[31] X. Gonze and C. Lee, Phys. Rev. B **55**, 10355 (1997).
[32] G.-M. Rignanese, X. Gonze, and A. Pasquarello, Phys. Rev. B **63**, 104305 (2001).
[33] Q. Wei and X. Peng, Appl. Phys. Lett. **104**, 251915 (2014).
[34] M. Klintenberg, S. Lebegue, C. Ortiz, B. Sanyal, J. Fransson, and O. Eriksson, J. Phys.: Condens. Matter **21**, 335502 (2009).
[35] S. Appalakondaiah, G. Vaitheeswaran, S. Lebègue, N. E. Christensen, and A. Svane, Phys. Rev. B **86**, 035105 (2012).
[36] J. F. Nye, *Physical Properties of Crystals* (Clarendon Press, Oxford, 1957).
[37] According to Voigt notation, the indices are contracted according to 11 →1, 22 →2, 11 →1, 33 →3, 23(32) →4, 13(31) →5, 12(21) →6, so that $e_{16}^{2D} = e_{112}^{2D} = e_{121}^{2D}$, $e_{25}^{2D} = e_{223}^{2D} = e_{232}^{2D}$, and so on.
[38] R. Fei, W. Li, J. Li, and L. Yang, Appl. Phys. Lett. **107**, 173104 (2015).
[39] P. Labéguerie, M. Harb, I. Baraille, and M. Rérat, Phys. Rev. B **81**, 045107 (2010).